SCIENTIFIC REPORTS
nature research

OPEN

Bulk-like dielectric and magnetic properties of sub 100 nm thick single crystal Cr_2O_3 films on an epitaxial oxide electrode

N. M. Vu[1], X. Luo[2], S. Novakov[2], W. Jin[3], J. Nordlander[4], P. B. Meisenheimer[1], M. Trassin[4], L. Zhao[2] & J. T. Heron[1]✉

The manipulation of antiferromagnetic order in magnetoelectric Cr_2O_3 using electric field has been of great interest due to its potential in low-power electronics. The substantial leakage and low dielectric breakdown observed in twinned Cr_2O_3 thin films, however, hinders its development in energy efficient spintronics. To compensate, large film thicknesses (250 nm or greater) have been employed at the expense of device scalability. Recently, epitaxial V_2O_3 thin film electrodes have been used to eliminate twin boundaries and significantly reduce the leakage of 300 nm thick single crystal films. Here we report the electrical endurance and magnetic properties of thin (less than 100 nm) single crystal Cr_2O_3 films on epitaxial V_2O_3 buffered Al_2O_3 (0001) single crystal substrates. The growth of Cr_2O_3 on isostructural V_2O_3 thin film electrodes helps eliminate the existence of twin domains in Cr_2O_3 films, therefore significantly reducing leakage current and increasing dielectric breakdown. 60 nm thick Cr_2O_3 films show bulk-like resistivity (~ 10^{12} Ω cm) with a breakdown voltage in the range of 150–300 MV/m. Exchange bias measurements of 30 nm thick Cr_2O_3 display a blocking temperature of ~ 285 K while room temperature optical second harmonic generation measurements possess the symmetry consistent with bulk magnetic order.

Magnetoelectric and multiferroic heterostructures have been of interest due to their potential for low-power, non-volatile spintronic devices utilizing the electric field control of magnetism[1–7]. Antiferromagnetic Cr_2O_3 is a promising candidate for such applications. It is one of the few single-phase materials that demonstrates an uncompensated surface magnetization that is switchable by its intrinsic magnetoelectric effect at room-temperature[3,8]. This materials configuration opens a diverse set of ways to create energy efficient spintronic devices[8–15].

One issue hindering electric field manipulation of magnetic order in thin film Cr_2O_3 is the existence of twin domain boundaries that result from the growth on elemental metal electrodes, particularly in films below 250 nm[12] which are necessary for technological adoption. The relatively conductive twin boundaries lead to high leakage current and reduce dielectric breakdown voltage down below the critical magnetoelectric switching voltage. In previous reports, this issue has been circumvented by utilizing Cr_2O_3 films of large thickness[12,16] but at proposed device scales this is not a viable solution. Using a V_2O_3 electrode layer, a metallic oxide isostructural with Cr_2O_3, has been shown to reduce or even eliminate twin domains and thereby reduce the leakage current of a 300 nm thick Cr_2O_3 film in comparison with metal electrodes[8,17]. In this work, we investigate the DC dielectric and magnetic properties of very thin (30–60 nm) single crystalline Cr_2O_3 films on V_2O_3 thin film electrodes at room temperature. Leakage data shows robust bulk like behavior for 60 nm thick samples with electrodes below 60 μm in diameter and 6–8 orders of magnitude lower leakage current than twinned Cr_2O_3 films grown on (111)-oriented Pt electrodes. Finally, investigation of the magnetic properties of single crystal Cr_2O_3 thin films using an exchange coupled ferromagnetic layer and optical second harmonic generation indicates bulk like behavior around room temperature in films at 30 nm thickness.

[1]Department of Materials Science and Engineering, University of Michigan, Ann Arbor, MI 48109, USA. [2]Department of Physics, University of Michigan, Ann Arbor, MI 48109, USA. [3]Department of Physics, Auburn University, Auburn, AL 36849, USA. [4]Department of Materials, ETH Zürich, Vladimir-Prelog-Weg 4, 8093 Zurich, Switzerland. ✉email: jtheron@umich.edu

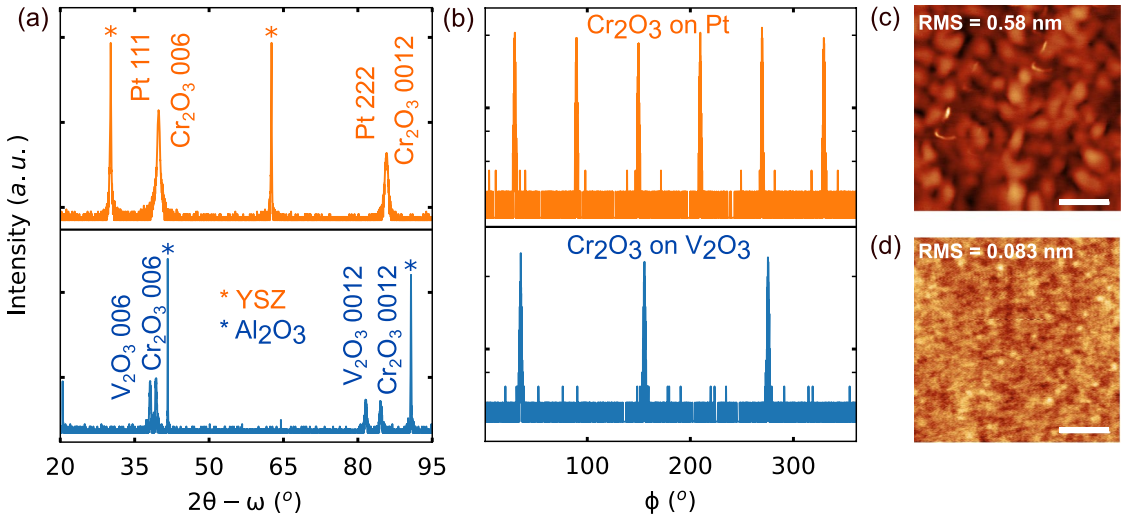

Figure 1. Synthesis of single crystalline Cr_2O_3 thin films on V_2O_3 electrodes. (**a**) $2\theta - \omega$ X-ray diffraction scans illustrating phase purity and the (0001) orientation of 70 nm thick Cr_2O_3 films on (111)-oriented Pt (40 nm)/Ti (4 nm)/YSZ (red) and 30 nm thick Cr_2O_3 films on (0001)-oriented V_2O_3 (30 nm)/Al_2O_3 (blue). (**b**) ϕ-scans of the {014} peaks of Cr_2O_3 reveal the in-plane twinning of the films on Pt/Ti buffered YSZ and single crystallinity on the V_2O_3 buffered Al_2O_3. (**c**,**d**) AFM topographs of Cr_2O_3/Pt/Ti/YSZ and Cr_2O_3/V_2O_3/Al_2O_3. Scale bar: 500 nm. The y-scale for X-ray diffraction data is logarithmic.

Results and discussions

Pulsed laser deposition. Our samples consist of epitaxial Al_2O_3 (0001)/V_2O_3 (30 nm)/Cr_2O_3 (30 to 60 nm) and YSZ (111) (Y_2O_3 stabilized ZrO_2, 8% mole Y_2O_3)/Ti (4 nm)/Pt (40 nm)/Cr_2O_3 (~70 nm) heterostructures. X-ray diffraction (XRD) 2θ-ω scans (Fig. 1a) show phase purity over the scan range and reveal the orientation of the layers. ϕ-scans of the Cr_2O_3{014} planes were then performed to confirm the presence of Cr_2O_3 on the Pt layer and the in-plane crystallinity. The ϕ-scan of the {014} planes will possess three-fold rotational symmetry for single crystal Cr_2O_3, thus could not only reveal in-plane film orientation but also identify the single crystal versus twinned nature. As shown in Fig. 1b, the ϕ-scans present three peaks for Cr_2O_3 on V_2O_3 and six peaks for Cr_2O_3 on Pt, which illustrates a single crystalline Cr_2O_3 film and a twinned Cr_2O_3 film with 60° in-plane domain rotations, respectively. The surface topography of the films shows a smooth surface for Cr_2O_3 grown on V_2O_3 (RMS = 0.083 nm) and grainy features for Cr_2O_3 grown on Pt (RMS = 0.58 nm) in Fig. 1c,d, respectively. It is important to have a single crystal Cr_2O_3 as the crystallographic twin domain boundaries lower the bandgap and results in a reduced breakdown voltage which hinders the electrical switching of the surface magnetization[12,16]. We then evaluate the electrical properties of twinned and single crystal Cr_2O_3 films with sub 100 nm thickness to illustrate this improvement.

Electrical characterizations. Figure 2a plots the mean resistivity of 60 and 30 nm thick Cr_2O_3 on V_2O_3/Al_2O_3 along with 70 nm thick Cr_2O_3 on Pt/Ti/YSZ. The mean resistivity at a given electrode size is determined from leakage current measurements of 24 to 25 different capacitors. Error bars represent one standard deviation. Supplementary Figure S1 shows all of the individual data points. The electrode diameters range from 45 to 95 μm. The resistivity of 60 nm thick single crystal Cr_2O_3 is ~ 10^{12} Ω cm and comparable to the bulk value[18] (dashed black line 10^{12} Ω cm) and is significantly higher than that of the twinned Cr_2O_3. When varying the thickness of single crystal Cr_2O_3, the leakage current increases with decreasing thickness. Increasing the electrode area leads to an increase in the number of leaky capacitors which can be accounted for by the increase in probability of encountering a defect. Twinned Cr_2O_3 grown on Pt exhibits poor resistivity performance even compared to single crystal Cr_2O_3 at lower thickness (30 nm) demonstrating significant improvement of thin film performance when twin domain boundaries are absent.

To further test the dielectric quality of single crystal Cr_2O_3 thin films on V_2O_3, electrical breakdown tests were performed with capacitors that have high resistivity at different electrode diameters (Fig. 2b). 60 nm thick Cr_2O_3 on V_2O_3 exhibits a high breakdown field (~ 170 to 225 MV/m—Fig. 2b), which is comparable to previously reported values (200 MV/m) for 500 nm thick Cr_2O_3 thin films with 200 × 200 μm electrodes[12], which is ~ 20% of the bulk breakdown field (1,000 MV/m)[16]. These values, however, are 3 × higher than the breakdown fields observed in the Cr_2O_3/Pt heterostructures containing twin domains. Dielectric breakdown of 30 nm thick single crystal Cr_2O_3 happens at slightly lower values when compared to thicker films (~ 90 to 160 MV/m) yet remains higher than that observed in the thicker and twinned Cr_2O_3/Pt heterostructures.

Magnetic properties. We next consider the magnetic properties of the single crystal Cr_2O_3 films. To probe the intrinsic magnetic and magnetoelectric order of the 30 nm single crystal Cr_2O_3 thin film on V_2O_3 at room temperature, we employed transmission optical second harmonic generation (SHG) measurements (Fig. 3a).

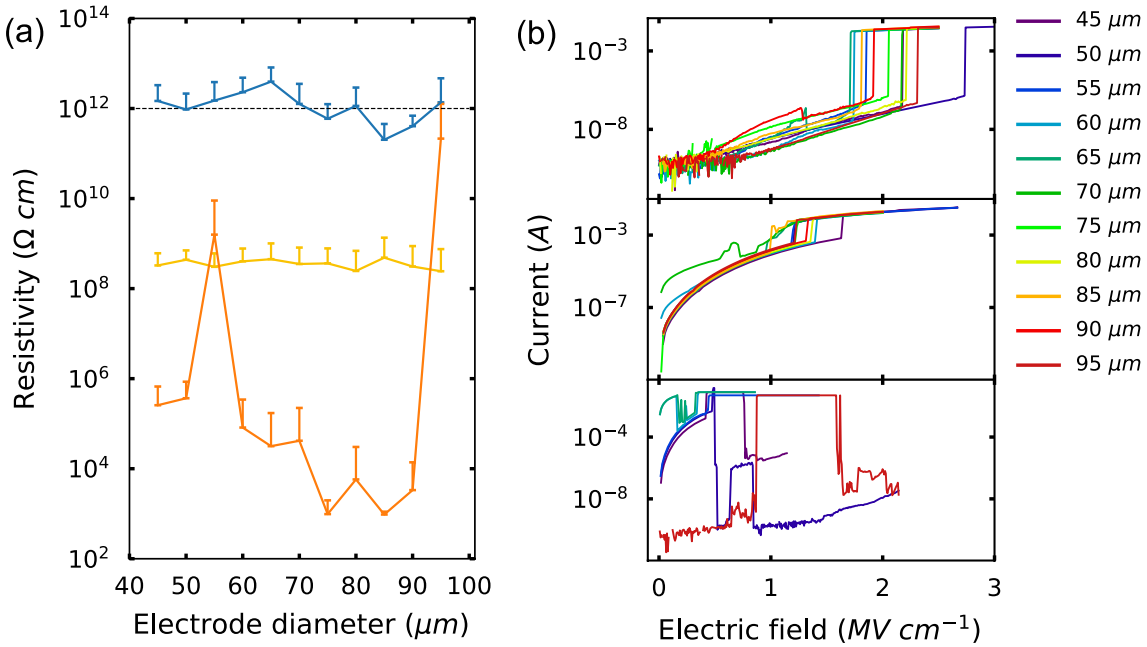

Figure 2. Electrical properties of Cr_2O_3 thin films on V_2O_3 electrodes. (**a**) Mean resistivity of 60 nm thick Cr_2O_3 (blue), 30 nm thick Cr_2O_3 (yellow) on (0001)-oriented V_2O_3/Al_2O_3 and 70 nm thick Cr_2O_3 on (111)-oriented Pt/Ti/YSZ (orange). 60 nm thick single crystal Cr_2O_3 reaches the bulk resistivity values (dashed black line). Error bars represent the standard deviation. (**b**) Electrical breakdown of low leakage devices in 60 nm thick Cr_2O_3 (top panel), 30 nm thick Cr_2O_3 on V_2O_3/Al_2O_3 (middle panel), and 70 nm thick Cr_2O_3 on Pt/Ti/YSZ (bottom panel) at different electrode diameters.

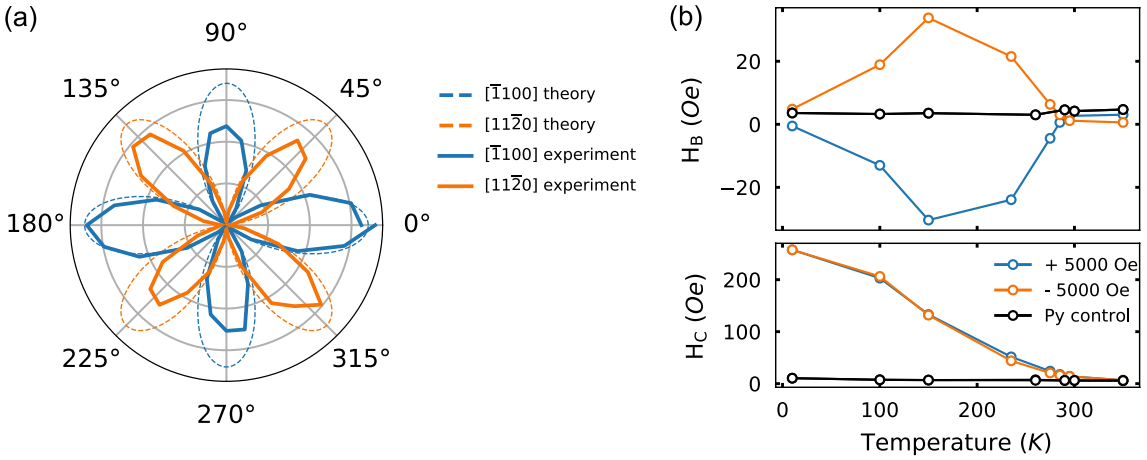

Figure 3. Magnetic characterization of Cr_2O_3 thin films on V_2O_3 electrodes. (**a**) Optical second harmonic generation intensity from 30 nm thick Cr_2O_3 on V_2O_3 electrode at room temperature (orange: analyzer along the x-direction ($[11\bar{2}0]$), blue: analyzer along y-direction ($[\bar{1}100]$)) and theoretical plot of electric dipole signal (Eq. (1b)) when analyzer is fixed along x-direction (dash-orange) and y-direction (dash-blue) showing the agreement between experimental result and theory. (**b**) Exchange bias field (top panel) and coercive field (bottom panel) as a function of temperature from Pt (5 nm)/Permalloy (Py) (4 nm)/Cr_2O_3 (30 nm)/V_2O_3/Al_2O_3 and Pt (5 nm)/Py (4 nm)/Al_2O_3 (labeled Py control) heterostructures. The Py control data shows both ± 5,000 Oe field cool scans.

Below the Néel temperature, bulk Cr_2O_3 possesses the magnetic point group $\bar{3}'m'$ that allows the existence of both magnetic (χ_m) and electric (χ_e) dipole susceptibility tensors[19–21]. The magnetic and electric contributions to SHG signals can be expressed as:

$$I_{MD} \propto \left| -\chi_m E_i^2 (\cos 2\,\phi_i \sin\,\phi_s + \sin 2\,\phi_i \cos\,\phi_s) \right|^2 \tag{1a}$$

$$I_{ED} \propto \left| -\chi_e E_i^2 (\sin 2\,\phi_i \sin\,\phi_s - \cos 2\,\phi_i \cos\,\phi_s) \right|^2 \tag{1b}$$

where E_i is the electric field of the incident beam. When fixing the analyzer along the y-direction ($[\bar{1}100]$) (or x- ($[11\bar{2}0]$)), $\sin\phi_s$ (or $\cos\phi_s$) goes to 0, and therefore the SHG intensity signal coming from the magnetic (I_{MD}) and electric (I_{ED}) dipole contributions will follow $\sin^2(2\phi)$ (or $\cos^2(2\phi)$) and $\cos^2(2\phi)$ (or $\sin^2(2\phi)$), respectively. The existence of the magnetic dipole signal is attributed to centrosymmetric point group $\bar{3}$ m and is expected in single crystal bulk Cr_2O_3. The electric dipole signal, however, is a proof of the existence of non-centrosymmetric magnetic order and only exists below the Néel temperature. The rotational-anisotropy data presented in Fig. 3b, following the $\cos^2(2\phi)$ ($\sin^2(2\phi)$) dependence on the incident polarization ϕ when the SHG analyzer is fixed along the y-axis (x-axis), proves the presence of the electric dipole contribution to the SHG signal and confirms that 30 nm thick single crystal Cr_2O_3 films on V_2O_3 electrodes possess the magnetic symmetry consistent with the magnetic order in bulk Cr_2O_3 at room temperature.

Using interface exchange coupling with a thin (4 nm) Permalloy (Py) layer, we probe the blocking temperature of the exchange bias heterostructure to approximate the Néel temperature. Figure 3b shows exchange bias and coercive fields as a function of temperature after cooling from 350 to 10 K in a ± 5,000 Oe in-plane training field. As the SHG of our thin films is consistent with the c-axis antiferromagnetic anisotropy of bulk Cr_2O_3 thin films, the applied in-plane magnetic field while cooling the sample through the Néel temperature is expected to induce a slight canting of the Cr moments in-plane, consistent with the observed in-plane exchange coupling with Py (Supplementary Figure S2). The exchange bias and coercivity enhancement extracted from M(H) curves disappear at ~ 285 K and ~ 295 K, respectively. These data reveal a blocking temperature that is lower than the bulk Néel temperature (307 K), however, this measured blocking temperature is significantly higher than the blocking temperature of films with comparable and greater thickness reported in the literature[22,23]. The blocking temperature can be qualitatively explained using Meiklejohn-Bean model with the competition between interface exchange coupling (fJ_{eb}—where f is a factor between 0 and 1 and represents the degree of interface spin disorder and often assumed to be 1), and the product of magnetic anisotropy energy (K_{AF}) and thickness (t_{AF}) of the antiferromagnetic layer[22,24]. Thus the increase in blocking temperature might be a result of a change in the magnetic anisotropy energy due to the reduced epitaxial strain from the Al_2O_3 substrate[22], however, the measured blocking temperature maybe lower than the Néel temperature of the thin film. Regarding the low temperature behavior, the exchange bias is ~ 0 and begins to increase up to ~ 35 Oe at 150 K where afterward it begins to decrease with increasing temperature up to the blocking temperature. Meanwhile, the coercivity monotonically decreases with increasing temperature. It is reported that there is a change in the Cr_2O_3 crystal structure at low temperature that is thought to lead to an in-plane tilting of the magnetic order[9] or a structural rearrangement at the (0001) surface of Cr_2O_3[25,26] which then affects both its antiferromagnetic structure and surface magnetism. In the Meiklejohn-Bean model, the ratio ($R \equiv \frac{K_{AF}t_{AF}}{fJ_{eb}}$) determines the exchange bias and coercive field behavior[24]. The competition between the change in spin structure (affects K_{AF}, J_{eb}) and the surface reconstruction (affects J_{eb}, f) will directly impact the low temperature behavior of the exchange bias field. In order to clarify the situation, future work focusing on isolating these factors is needed.

Conclusion

In conclusion, by using V_2O_3 as an epitaxial buffer layer, crystallographic twinning of Cr_2O_3 thin films can be eliminated leading to near bulk dielectric and magnetic behavior in Cr_2O_3 films with thickness well below 100 nm. Leakage measurements performed on very thin single crystal Cr_2O_3 films, along with electric breakdown tests, as a function of capacitor area suggest the need to further improve film quality or develop additional dielectric layers to mitigate the dielectric parasitics observed at larger capacitor size and enable magnetoelectric characterization with transport methods. Our investigation of magnetic properties in 30 nm thick films indicate bulk magnetic and magnetoelectric order at room temperature and indicate that the magnetoelectric switching of very thin single crystal Cr_2O_3 films on V_2O_3 electrodes may be possible at room temperature.

Methods

Pulsed laser deposition. Samples are fabricated using pulsed laser deposition (PLD) with a 248 nm KrF Excimer laser with a pulse duration of ~ 25 ns using commercially available targets from (V_2O_5 99.9%, Cr_2O_3 99.9%). V_2O_3 is deposited onto a Al_2O_3 (0001) single crystal substrate at 400 °C from an V_2O_5 target with a fluence ~ 2.8 J/cm^2 and ~ 10 mTorr Ar background pressure. Cr_2O_3 is then deposited directly on the V_2O_3 film at 500 °C from a Cr_2O_3 target with a fluence ~ 2.2 J/cm^2 under 30 mTorr Ar background pressure. Pt is grown on a (111)-oriented YSZ substrate with a buffer layer of Ti for the purpose of adhesion[27]. Both Pt and Ti are deposited using metallic targets at 550 °C with a fluence ~ 3.6 J/cm^2 under 20 mTorr Ar gas. Cr_2O_3 is then also deposited directly on Pt at 700 °C with a fluence ~ 2.2 J/cm^2 under 30 mTorr O_2 background pressure. For testing the magnetic properties of our single crystal thin film, a 4 nm Permalloy (Py) film was then deposited on single crystal Cr_2O_3 grown on V_2O_3 and was capped with 5 nm of Pt for preventing oxidation. The Py and Pt metal layers are deposited at room temperature with a fluence ~ 3 J/cm^2 under 20 mTorr Ar gas.

As a Metal–Insulator-Transition material, the growth of V_2O_3 has been intensively discussed elsewhere[28–30]. The challenge, however, lies in finding compatible conditions for the growth of Cr_2O_3. We found that the presence of oxygen (10 mTorr) as the background gas causes the formation of V_2O_5. The V_2O_5 was found to melt even at a substrate temperature (650 °C) lower than its melting point (690 °C). Reduction of the substrate temperature in oxygen, however, favors the formation of the VO_2 phase. By switching to argon gas at the same temperature (400 °C), we achieved V_2O_3 thin films with desired topography, x-ray diffraction pattern, and resistivity. The substrate temperature for the growth of the Cr_2O_3 layer was chosen to achieve high crystallinity and low surface roughness while mitigating the oxidation of the underlying V_2O_3 layer from the oxygen in the ablation plume of the Cr_2O_3 target. We optimized our conditions for Cr_2O_3 growth on V_2O_3 starting from the conditions for high quality Cr_2O_3 growth on a bare Al_2O_3 substrate. At our deposition energy, Cr_2O_3 requires high temperature

(700 °C) to achieve good crystallinity. However, at that temperature, we speculate that there is a reaction happening at the interface between V_2O_3 and Cr_2O_3, since V_2O_3 is easy to be oxidized in the presence of oxygen, especially at elevated temperature. The growth temperature was therefore systematically reduced. These above conditions were selected after tuning deposition conditions using surface roughness from AFM and XRD measurements (Peak position, intensity, and oscillation fringes) were used to assess conditions and feedback the growth. From the presence of oscillation fringes around V_2O_3 peak, the quality is considered as comparable to previous report of a good crystallinity in thin film[30].

Circular Ti (6 nm)/Pt (120 nm) top electrode capacitors of diameter from 10 to 150 mμ were defined using a standard liftoff process and PLD deposition.

X-ray diffraction. $2\theta - \omega$ and ϕ scans were performed using a Rigaku Smart Lab diffractometer (Cu K_α radiation and equipped with a Ge (220) × 2 monochromator on the incident) side to assess the orientation and crystallinity of the films.

Atomic force microscopy. The surface topography of the films is observed using an NT-MDT NTEGRA atomic force microscope (AFM).

Magnetometry. Vibrating sample magnetometry was performed using a QuantumDesign Dynacool Physical Property Measurement System (PPMS).

Electrical measurements. Leakage currents through thin film Cr_2O_3 are investigated using a Radiant Technologies Precision Multiferroic II with minimum current detection of 1 pA for a 2 s integration period. An electric field of approximately 1.4 to 1.7 MV/m is applied to detect leakage current. Breakdown tests are performed using a Keithley 2420 with a detection limit of 500 pA. These measurements are performed at ambient conditions in a probe station using W tips with a tip diameter of 5 μm.

Second harmonic generation measurement. A rotational-anisotropy SHG measurement was performed with the beam at normal incidence. The transmitted SHG intensity is collected with a single photon count detector as a function of the azimuthal angle ϕ_i between the incident electric polarization and the in-plane crystalline axis $[11\bar{2}0]$ and the analyzer angle ϕ_s between the selected SHG electric polarization and the in-plane crystalline axis $[\bar{1}100]$. The incident ultrafast light source was of 800 nm wavelength, 40 fs pulse duration and 200 kHz repetition rate, and focused onto a 20 μm diameter spot on the sample with a fluence of ~ 0.25 mJ/cm^2.

Data availability

The data that support the findings of this study are available from the corresponding author upon reasonable request.

Received: 25 March 2020; Accepted: 18 August 2020
Published online: 07 September 2020

References

1. Spaldin, N. A. & Ramesh, R. Advances in magnetoelectric multiferroics. *Nat. Mater.* **18**(3), 203 (2019).
2. Liu, M. *et al.* Electrically controlled non-volatile switching of magnetism in multiferroic heterostructures via engineered ferroelastic domain states. *NPG Asia Mater.* **8**, e316–e316 (2016).
3. He, X. *et al.* Robust isothermal electric control of exchange bias at room temperature. *Nat. Mater.* **9**, 579–585 (2010).
4. Heron, J. T. *et al.* Deterministic switching of ferromagnetism at room temperature using an electric field. *Nature* **516**(7531), 370 (2014).
5. Chu, Y. H. *et al.* Low voltage performance of epitaxial $BiFeO_3$ films on Si substrates through lanthanum substitution. *Appl. Phys. Lett.* **92**, 102909 (2008).
6. Bibes, M. & Barthélémy, A. Towards a magnetoelectric memory. *Nat. Mater.* **7**, 425–426 (2008).
7. Meisenheimer, P. B., Novakov, S., Vu, N. M. & Heron, J. T. Perspective: Magnetoelectric switching in thin film multiferroic heterostructures. *J. Appl. Phys.* **123**, 240901 (2018).
8. Kosub, T. *et al.* Purely antiferromagnetic magnetoelectric random access memory. *Nat. Commun.* **8**, 13985 (2017).
9. Astrov, D. N. Magnetoelectric effect in chromium oxide. *J. Exp. Theor. Phys.* **13**, 729–733 (1961).
10. Martin, T. & Anderson, J. Antiferromagnetic domain switching in Cr_2O_3. *IEEE Trans. Magn.* **2**, 446–449 (1966).
11. Borisov, P., Hochstrat, A., Chen, X., Kleemann, W. & Binek, C. Magnetoelectric switching of exchange bias. *Phys. Rev. Lett.* **94**, 117203 (2005).
12. Ashida, T. *et al.* Isothermal electric switching of magnetization in Cr_2O_3 /Co thin film system. *Appl. Phys. Lett.* **106**, 132407 (2015).
13. Toyoki, K. *et al.* Magnetoelectric switching of perpendicular exchange bias in Pt/Co/α-Cr_2O_3/Pt stacked films. *Appl. Phys. Lett.* **106**, 162404 (2015).
14. Cheng, Y., Yu, S., Zhu, M., Hwang, J. & Yang, F. Evidence of the topological Hall Effect In Pt/antiferromagnetic insulator bilayers. *Phys. Rev. Lett.* **123**, 237206 (2019).
15. Dehn, M. H. *et al.* Observation of a charge-neutral muon-polaron complex in antiferromagnetic Cr_2O_3. *Phys. Rev. X* **10**, 011036 (2019).
16. Sun, C. *et al.* Local dielectric breakdown path along *c*-Axis Planar boundaries in Cr_2O_3 thin films. *Adv. Mater. Interfaces* **4**, 1700172 (2017).
17. Mahmood, A. *et al.* Dielectric properties of thin Cr_2O_3 films grown on elemental and oxide metallic substrates. *Phys. Rev. Mater.* **2**, 044401 (2018).
18. Kwan, C.-P., Chen, R., Singisetti, U. & Bird, J. P. Electric-field dependent conduction mechanisms in crystalline chromia. *Appl. Phys. Lett.* **106**, 112901 (2015).
19. Fiebig, M., Pavlov, V. V. & Pisarev, R. V. Second-harmonic generation as a tool for studying electronic and magnetic structures of crystals: Review. *J. Opt. Soc. Am. B* **22**, 96 (2005).

20. Fiebig, M., Fröhlich, D., Krichevtsov, B. B. & Pisarev, R. V. Second harmonic generation and magnetic-dipole-electric-dipole interference in antiferromagnetic Cr_2O_3. *Phys. Rev. Lett.* **73**, 2127–2130 (1994).
21. Nordlander, J., De Luca, G., Strkalj, N., Fiebig, M. & Trassin, M. Probing ferroic states in oxide thin films using optical second harmonic generation. *Appl. Sci.* **8**, 570 (2018).
22. Shimomura, N., Pati, S. P., Nozaki, T., Shibata, T. & Sahashi, M. Enhancing the blocking temperature of perpendicular-exchange biased Cr_2O_3 thin films using buffer layers. *AIP Adv.* **7**, 025212 (2017).
23. Nozaki, T. *et al.* Large perpendicular exchange bias and high blocking temperature in Al-doped Cr_2O_3/Co thin film systems. *Appl. Phys. Exp.* **10**, 073003 (2017).
24. Radu, F. & Zabel, H. Exchange bias effect of ferro-/antiferromagnetic heterostructures. In *Magnetic Heterostructures* 97–184 (Springer, Berlin, 2008). https://doi.org/10.1007/978-3-540-73462-8_3.
25. Freund, H.-J., Kuhlenbeck, H. & Staemmler, V. Oxide surfaces. *Rep. Prog. Phys.* **59**, 283 (1996).
26. Kleemann, W. & Binek, C. Multiferroic and magnetoelectric materials. In 163–187 (2013). https://doi.org/10.1007/978-3-642-32042-2_5.
27. Trassin, M. *et al.* Ultraflat monocrystalline Pt (111) electrodes. *J. Appl. Phys.* **105**, (2009).
28. Brockman, J. S. *et al.* Subnanosecond incubation times for electric-field-induced metallization of a correlated electron oxide. *Nat. Nanotechnol.* **9**, 453–458 (2014).
29. Sakai, J., Limelette, P. & Funakubo, H. Transport properties and c/a ratio of V_2O_3 thin films grown on C- and R-plane sapphire substrates by pulsed laser deposition. *Appl. Phys. Lett.* **107**, 241901 (2015).
30. Thorsteinsson, E. B., Shayestehaminzadeh, S. & Arnalds, U. B. Tuning metal-insulator transitions in epitaxial V_2O_3 thin films. *Appl. Phys. Lett.* **112**, 161902 (2018).

Acknowledgements

This work was funded in part by IMRA America. This work was performed in part at the University of Michigan Lurie Nanofabrication Facility. This work was supported in part by the Semiconductor Research Corporation (SRC) as the NEWLIMITS Center and NIST through award number 70NANB17H041. L. Zhao acknowledges support by NSF CAREER Grant No. DMR-1749774. P.B.M and J.T.H. acknowledge support by NSF CAREER Grant No. DMR-1847847.

Author contributions

N.V. fabricated the films, performed electrical measurements and magnetometry. S.N. performed lithography processes. X.L., W.J., J.N., P.M. performed the SHG measurements. J.H., L.Z., M.T. planed the research. N.V. and J.H. wrote the manuscript.

Competing interests

The authors declare no competing interests.

Additional information

Supplementary information is available for this paper at https://doi.org/10.1038/s41598-020-71619-1.

Correspondence and requests for materials should be addressed to J.T.H.

Reprints and permissions information is available at www.nature.com/reprints.

Publisher's note Springer Nature remains neutral with regard to jurisdictional claims in published maps and institutional affiliations.